



# Terahertz waveguiding in glass-clad silicon wafers

TRYGVE SØRGÅRD,<sup>1</sup>  KJELL MARTIN MØLSTER,<sup>2</sup> FREDRIK LAURELL,<sup>2</sup> VALDAS PASISKEVICIUS,<sup>2</sup> URSULA J. GIBSON,<sup>1,2,\*</sup>  AND ULF L. ÖSTERBERG<sup>2,3</sup>

<sup>1</sup>Department of Physics, Norwegian University of Science and Technology, Trondheim NO-7491, Norway

<sup>2</sup>Department of Applied Physics, Royal Institute of Technology, KTH, 10691 Stockholm, Sweden

<sup>3</sup>Department of Electronic Systems, Norwegian University of Science and Technology, N-7491 Trondheim, Norway

\*[ursula.gibson@ntnu.no](mailto:ursula.gibson@ntnu.no)

**Abstract:** The waveguiding properties of high-resistivity float zone silicon slab waveguides are characterized over the spectral range from 0.5 to 7.5 THz. Waveguide modes and dispersion are observed for lengths of 1.2 cm and silicon thicknesses from 40 to 300  $\mu\text{m}$ . The influence of core thickness and cladding glass attenuation is characterized, and modeled transmitted pulse shapes compare well to the measured signals. Fused silica cladding allows propagation in the 40  $\mu\text{m}$  thick wafer, demonstrating the feasibility of developing flexible semiconductor core fibers for THz transmission.

© 2020 Optical Society of America under the terms of the [OSA Open Access Publishing Agreement](#)

## 1. Introduction

The spectroscopic signatures of materials in the THz band (0.1 – 10 THz) are of interest for communications, medical and security and materials science [1] applications, but their exploitation is limited by strong absorption in humid air. Waveguides, in particular flexible fibers, are therefore of great practical importance for signal delivery and collection, and propagation of broadband single-cycle THz pulses has been demonstrated in a variety of different systems. Hollow metallic waveguides [2,3], metal surfaces [4–8], sapphire fibers [9], polymers [10–18], and polymer tubes with dielectric coatings [19,20], have been investigated, along with different forms of silicon (Si), such as ribbons [21], photonic crystals [22,23], and crystals with metallic coatings [24]. Most of these studies were performed below 1.1 THz, but high resistivity float-zone (HRFZ) Si has been found to be transparent and virtually free of dispersion through the THz band [25]. It is therefore considered a prime candidate as a core material for dielectric waveguides.

Recently, semiconductor core optical fibers have emerged as flexible infrared (IR) waveguides [26–28] suggesting their potential as THz waveguides for applications including endoscopy [29,30], communications and imaging [1]. Modeling results for THz transmission through semiconductor core fiber [26] suggest that molten-core drawing is a scalable technology for the production of THz waveguides. In such models, the glass cladding has the potential to significantly affect transmission when waveguide dimensions are small enough for the electric field to extend outside the core. For example, in a planar analog, borosilicate glass, with a high THz absorption coefficient [31], was etched away from under the guiding channel in a silicon-on-glass waveguide to reduce the losses [23]. Fused silica, with lower absorption in the THz-regime [31], is more promising as a cladding material.

This paper extends the frequency range over which silicon transmission is reported, and includes the first experimental data on semiconductor/glass core/cladding waveguide systems. It sets the stage for future THz silicon-core fiber design by characterization of materials suitable for fiber production, but in a slab waveguide configuration that permits independent control of the materials and geometry. Low loss HRFZ Si wafers with thicknesses of 40 to 300  $\mu\text{m}$  were used

as the core material, and the cladding glasses investigated were fused silica and soda lime glass, known to have significantly different absorption coefficients [31,32]. As the thickness of the core is reduced, the influence of the cladding glass becomes more apparent. Waveguiding properties of these materials combinations were tested using broadband THz Time-domain transmission spectroscopy.

## 2. Experimental and modeling methods

The THz reflection and transmission setup, enclosed in a plexiglass box which was dehumidified with calcium sulfate (VWR Drierite) to a level less than 5% relative humidity at room temperature (measured using a ITHX-SD-5, OMEGA) is shown in Fig. 1(a). The spectroscopy system is based on a Ti:Sapphire laser (Spectra-Physics, Solstice) with a central wavelength of 798 nm, an average power of 3 W, 1 kHz repetition rate, and 90 fs pulse width. The IR beam was split with 99% used as the pump for THz generation (thick red line), and the remaining power used as a probe (thin red line). The pump passes through a  $\beta$ -Barium borate crystal (BBO) to create a second harmonic pulse (thick blue line). When the second harmonic and the residual fundamental are focused together in air, a two-color plasma interaction generates single-cycle THz pulses (light blue shading) [33]. The IR and the visible are filtered out using a high-reflection (HR)-coated Si wafer (TYDEX) and the transmitted THz pulses pass through a high density polyethylene polarizer (TYDEX). The chopper provides the reference frequency for the detection lock-in amplifier (SR830, Stanford Research Systems). Two parabolic mirrors collect and focus the THz radiation onto a gold mirror, and it then passes through a polymethylpentene (TPX) lens (focal length = 10 mm, Batop). The waveguide is placed near the focal plane of the lens permitting signal optimization and sample exchange with minimal disturbance of the system configuration. The probe beam, which combines with the THz for detection, passed through a retro-reflector on a motorized delay stage (IMS-LM, Newport) and is directed through a [110]-cut gallium phosphide (GaP) crystal from the detector side, since the Si core of the waveguide is opaque at 798 nm. There is an IR anti-reflective (AR) coating on this side of the crystal, but significant reflection occurs on the uncoated (sample) side of the crystal to give an IR probe co-propagating with the THz beam. The GaP thickness (300  $\mu\text{m}$ ) optimizes phase matching, but serves as a systemic upper bound for the resolution of measured dispersion, since sequential pulses will interfere if the pulse duration exceeds 6 ps. The THz field rotates the polarization of the reflected probe pulse inside the GaP crystal and a balanced photodetector (Zomega) is used to detect the polarization shift while the delay between the IR and THz signals is scanned by the motorized stage. Figure 1(b) shows a time-trace of the reference THz signal in the absence of a waveguide. The time-scale is relative to the position of the delay stage, with the shortest possible path-length for the probe beam set to time  $t = 0$ . Samples were assembled from double-side polished <100> HRFZ Si wafers (purchased through El-Cat, Inc) with thicknesses of  $40 \pm 15$ ,  $160 \pm 25$ , and  $300 \pm 25$   $\mu\text{m}$ , sandwiched between different 1 mm thick glass slides to form a dielectric-clad planar waveguide. Soda lime glass microscope slides (VWR) were used as a cladding for all three thicknesses, and fused silica plates (UQG Optics) were used for the thinner waveguides. An acrylic adhesive was applied to the side faces to hold the assemblies together, as shown in the inset of Fig. 1. Samples were 11.10 to 12.50 mm long and were 4 – 6 mm wide to ensure the glued edges were beyond the THz beam.

Fourier transforms of the measured time signals were performed to obtain the frequency spectrum. As the infrared AR coating does not eliminate the reflections of the THz pulses, a series of dispersed pulses separated by the average optical thickness of the GaP in the THz regime - 6 ps - is detected (Fig. 1(b)). Including the pulse train in the Fourier transform adds a periodic ringing to the spectrum as seen in Fig. 1(c). The periodic ringing can be eliminated by selection of a time window that includes only one pulse. However, this was not done in all cases as the

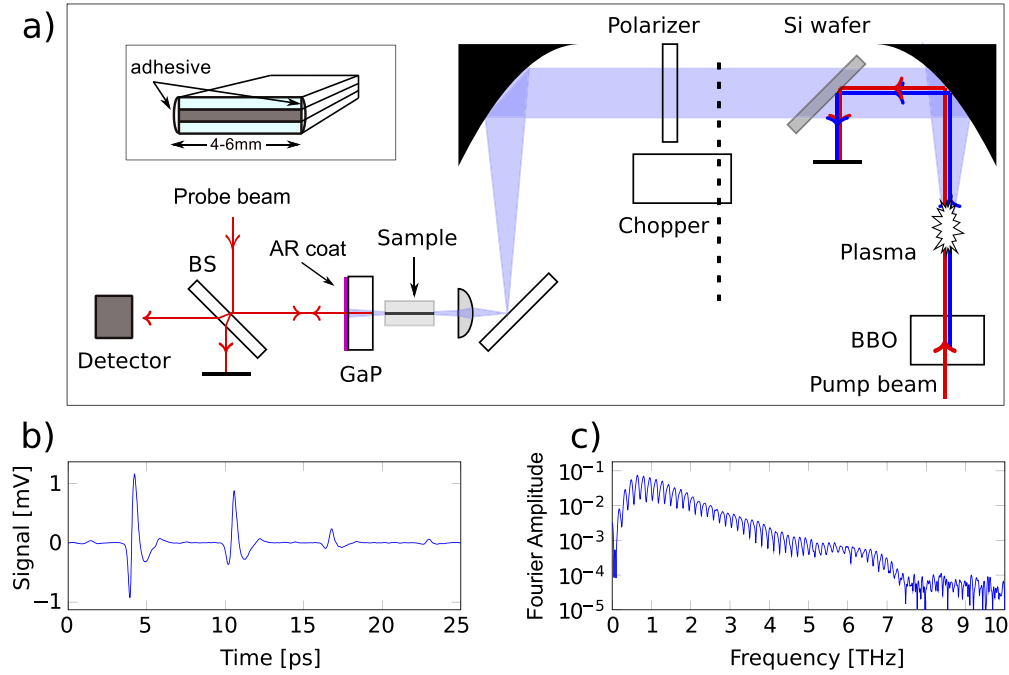


**Fig. 1.** THz spectroscopy; a) experimental setup (inset shows sample geometry). b) Reference time-signal in the absence of a waveguide. The successive pulses are Fabry-Pérot echoes from the GaP crystal. c) Corresponding frequency spectrum.

ringing is an indicator of experimental conditions (note these features are less well defined from 5-7 THz, even in the absence of a sample).

Modeling of the waveguide behavior was performed using a minimum number of adjustable parameters, and we assume that the fundamental mode of the waveguide dominates the throughput signal (see appendix). The theoretical propagation through a waveguide can be expressed as

$$E_{out}(\nu) = E_{ref}(\nu)C^2T \exp\{-ik_0(n_{eff}(\nu) - 1)z\} \exp\{-k_0\kappa_{eff}(\nu)z\}, \quad (1)$$

where  $E_{ref}(\nu)$  is the Fourier transform of the first pulse of the reference signal (from Fig. 1(b)),  $T$  is the transmittance, accounting for reflections at the input and output ends,  $C^2$  is the overlap integral of the input and output beams and the fundamental mode. For simplicity, we assume that  $C^2$  is equal for all frequencies.  $\hat{n}_{eff}(\nu) = n_{eff}(\nu) - i\kappa_{eff}(\nu)$  is the calculated complex effective refractive index of the waveguide,  $z$  is the measured length of the waveguide, and  $k_0$  is the wavenumber in air. In the calculations, the adjustable parameters were  $C^2$ , and sample dimensions (within the measurement uncertainties). Changing the sample thickness led to changes in the calculated effective refractive index, and thereby the dispersion while the length affects the delay time.

The simulations used Fourier transforms of the first reference pulse seen in Fig. 1(b) to get  $E_{ref}(\nu)$ . A finite difference solver written in MATLAB was used to calculate  $n_{eff}(\nu)$  for all frequencies within the experimental bandwidth. The inverse Fourier transform of  $E_{out}(\nu)$  yields the simulated signal in the time domain. Si was assumed to be non-dispersive, with  $n = 3.42$  over the entire bandwidth. The transparency of Si is heavily dependent on the concentration of free-carriers, but based on our spectroscopic measurements of the Si wafers we set the extinction coefficient,  $\kappa = 2 \cdot 10^{-4}$  as an upper limit of the absorption. This agrees well with earlier measurements of HRFZ Si [34,35]. The fused silica cladding was modeled following Naftaly and

Miles [31], who measured the optical properties of different glasses from 0.1 to 2.0 THz. They characterized the relation between the refractive index  $n(\nu)$  and absorption coefficient  $\alpha(\nu)$  as

$$\alpha(\nu) = \frac{Kh^2\nu^\beta}{n(\nu)} \quad (2)$$

with absorption increasing as frequency to the power of  $\beta$  in the bulk glass. For fused silica, they found  $n(\nu) = 1.96 \pm 0.01$ ,  $Kh^2 = 5 \pm 1 \text{ cm}^{-1}\text{s}^2$ ,  $\beta = 2.0 \pm 0.1$ . They attributed the absorption in different glasses to the presence of ionic alkali oxides; as soda lime glass typically contains only 70%  $\text{SiO}_2$ , it has higher absorption than pure silica. The values for refractive index and absorption for soda lime glass were taken from [32], and the index is substantially higher ( $n(1 \text{ THz}) = 2.608$ ) than that for silica. The absorption in the waveguide configuration has a peak at low frequencies due to the absorptive cladding. As the wavelength becomes small in comparison to the waveguide dimensions, the Si core becomes the primary contributor to absorption.

### 3. Results and discussion

Experiments were performed to determine the behavior that can be expected from glass clad waveguides, in a system where the Si quality, surface roughness, waveguide thickness and cladding properties can be independently controlled. The modal, absorptive, and spectral properties of the guides were assessed. First, we confirm that the samples are long enough for mode establishment by coupling to the TE and TM modes of a 300  $\mu\text{m}$  thick waveguide. Second, we show how the choice of glass impacts dispersion and absorption, by coupling into 160  $\mu\text{m}$  thick waveguides with different cladding materials. Finally, we show that with fused silica cladding, unequivocal transmission out to 4.5 THz is observed for a 40  $\mu\text{m}$  Si wafer, where a significant amount of energy lies outside the core.

Figure 2 shows the transmitted signal through perpendicular orientations of the same sample, a 300  $\mu\text{m}$  thick Si wafer with soda lime cladding, length  $12.00 \pm 0.05 \text{ mm}$ , along with simulations based on the glass data of Rubin [32]. The sample was placed with the wafer parallel and perpendicular to the THz polarization, coupling the TE and TM modes. Both show anomalous dispersion associated with the waveguide structure. There is a clear difference between the two modes, with the TE being less dispersed than the TM mode, following waveguide theory. The TM mode arrives slightly earlier in time than the TE-mode, but this difference ( $<0.5 \text{ ps}$ ) is attributed to length variation in the hand-polished sample. The agreement with simulation confirms that the fundamental mode dominated the throughput signal. The simulations assume coupling of  $C^2 = 1$  for each frequency after Fresnel losses. The experimental data suggests the coupling is less efficient for the lower frequencies, as seen by the discrepancy between experimental and simulated values in the later part of the time-trace. This may be due to focusing errors. The simulation used a thickness of 295  $\mu\text{m}$  and lengths of 11.98 and 11.95 mm for the TE and TM modes, which correlated well with measured values.

The corresponding spectra of the two measurements (single pulse Fourier Transforms), are shown in Fig. 3. The entire spectral content is transmitted, but the TM mode suffers from slightly higher absorption, most noticeable below 4.5 THz, where the longer wavelengths result in modes that extend further into the cladding glass. The differences between absorption for the modes decreases with frequency, as the impact of the cladding is reduced.

The next set of measurements were made on 160  $\mu\text{m}$  thick wafers, where cladding glass absorption differences should be detectable. The samples were measured in the TE configuration to reduce sequential pulse overlap due to dispersion. The soda lime clad sample was measured to be  $12.30 \pm 0.05 \text{ mm}$  long, and the fused silica sample was  $11.65 \pm 0.10 \text{ mm}$  long. Figure 4 shows the time-traces for the two samples, and very good agreement between experiments and simulations can be seen. The simulation shown was obtained with a thickness of 165  $\mu\text{m}$  and length 11.70 mm for the fused silica, and a thickness of 155  $\mu\text{m}$  and length 12.30 mm for the

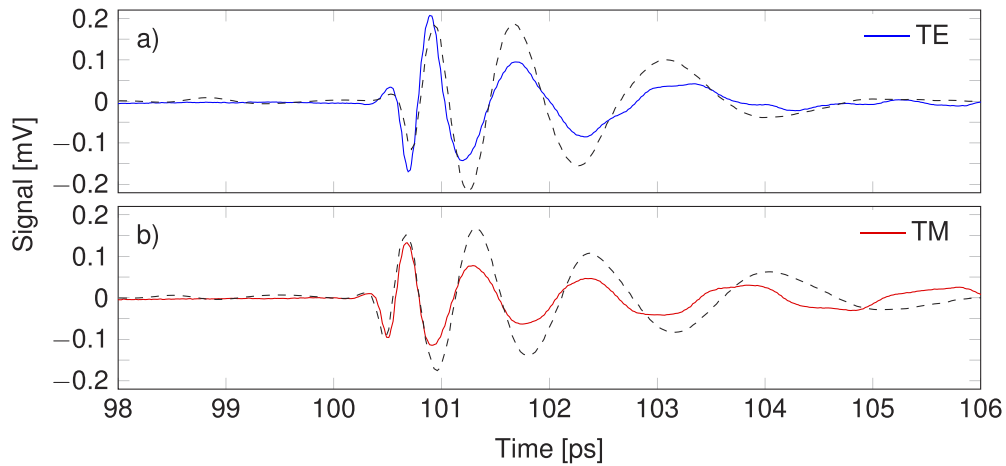


**Fig. 2.** Time traces of the THz pulse transmitted through different orientations of a 300  $\mu\text{m}$  thick waveguide with soda lime cladding, positioned to excite a) TE and b) TM modes. Solid lines are experimental data and dashed lines are simulations.

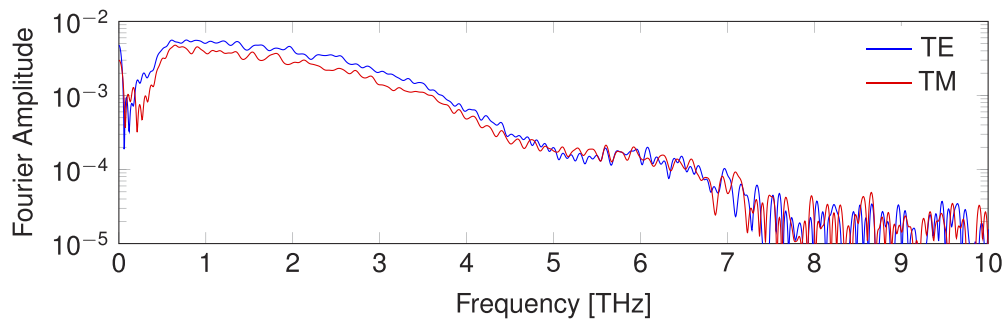


**Fig. 3.** Spectra of a 300  $\mu\text{m}$  thick waveguide with soda lime cladding for TE and TM modes.

soda lime glass, in accord with measured values. The model assumed a coupling coefficient of  $C^2 = 0.5$  for all frequencies to the fundamental mode. This value was chosen to fit the measured signal, and scales well with the wafer thickness. Small oscillations in the silica-clad sample before the main signal arrives are cladding modes able to propagate through the fused silica. The lengths and thicknesses used in the simulations in Figs. 2 and 4 were chosen to give the best fit for the dispersion, and are well within the experimental uncertainties of the waveguide dimensions. Fabry-Pérot echoes from reflections inside the GaP crystal are evident in the experimental data due to the extended time window, causing the ringing seen in Fig. 5. For the fused silica cladding, the difference between core and cladding refractive indices results in a dispersed signal that is elongated sufficiently to interact with the following THz reflection inside the GaP, even for the TE mode. The soda lime cladding has more absorption and a larger refractive index, resulting in less dispersion and a small separation between the echoes within the GaP.

Figure 5 shows the spectra of the 160  $\mu\text{m}$  thick waveguides. While both samples transmit up to 7.5 THz, we see that there is significantly more signal transmitted by the fused silica sample than the soda lime clad sample. Between 5 and 6.5 THz, there is a dip in signal strength for both samples. Analysis of the signal to noise (S/N) ratio for spectra taken under different conditions showed that there is a consistent reduction in the S/N in this region, possibly due to the details of the plasma generation, or variation in chamber humidity. Based on this S/N characterization, and

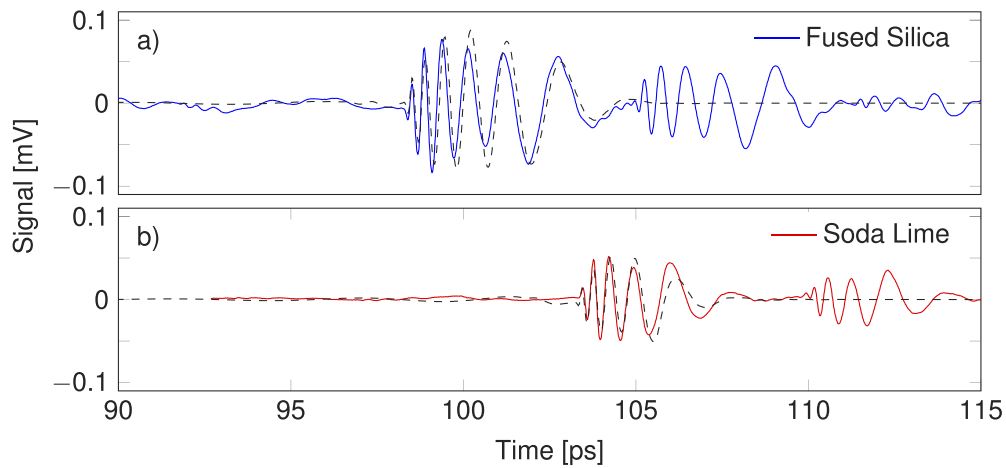


**Fig. 4.** Time trace of two 160  $\mu\text{m}$  thick Si waveguides with cladding of a) fused silica and b) soda lime glass. Solid lines are experimental data showing GaP echoes, dashed lines are simulations. Both samples were measured in the TE configuration.

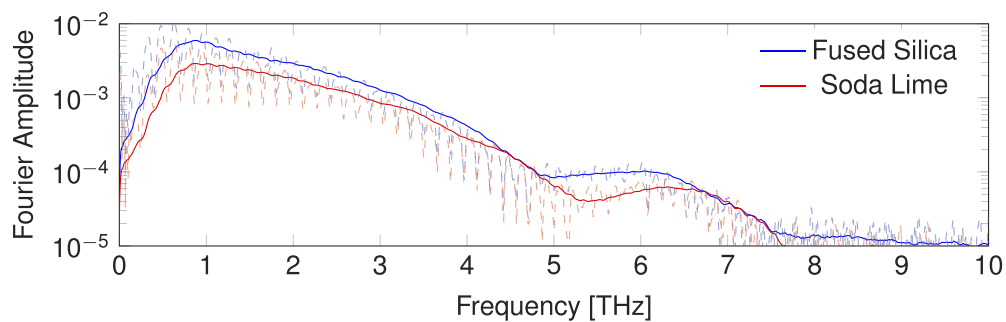
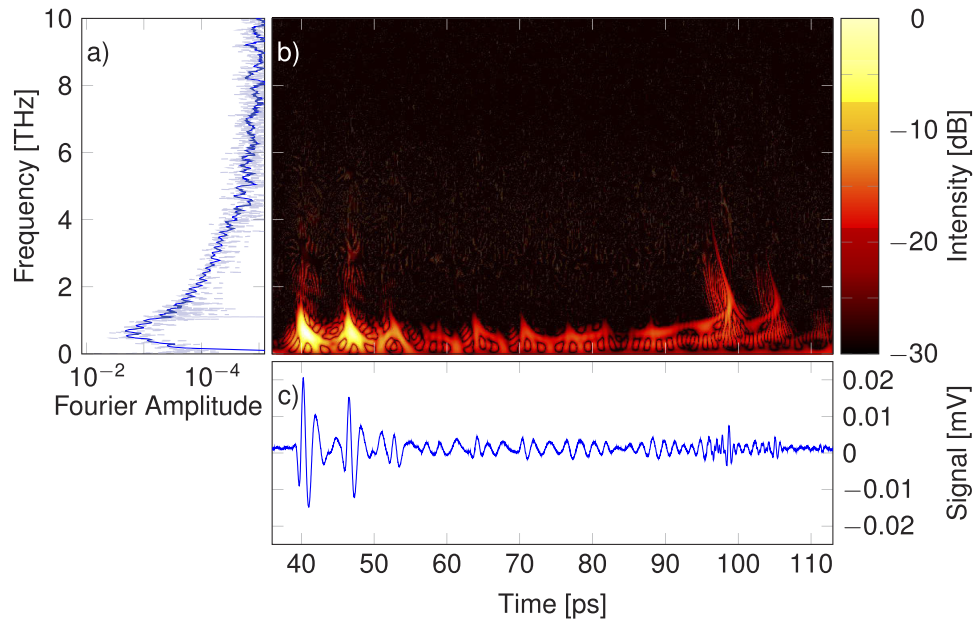


**Fig. 5.** Fourier amplitudes of 160  $\mu\text{m}$  thick waveguides with different claddings. The dotted lines show the Fabry-Pérot echoes. The thick lines show a smoothed average.

the loss of coherent Fabry-Pérot oscillations in that spectral window, the broad shoulder is likely dominated by experimental system variations rather than by material attenuation.

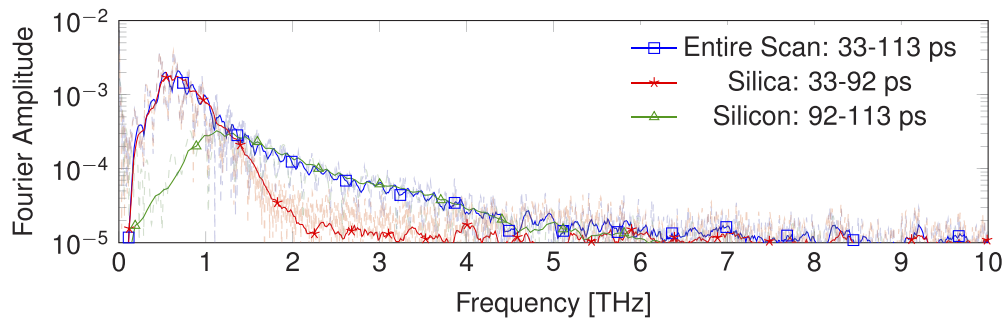
Figure 6 shows the spectral signal, Wigner-Ville transformation and the time-trace of the signal transmitted through a  $11.10 \pm 0.10$  mm long, 40  $\mu\text{m}$  thick, fused silica-clad Si wafer in the TE configuration. Since the cladding is much thicker than the core, and the core is smaller than the THz beam diameter, a large portion of the power is coupled into the cladding. Multiple oscillations are visible in the time-trace due to cladding modes, making it more challenging to find a signal. However, the rapid oscillations around 98 ps arrive at the expected time for Si transmission, and exhibit the anticipated chirp in the Wigner-Ville representation, evidenced by the curved shapes around 99 and 106 ps. In contrast, there was no detectable signal through a 40  $\mu\text{m}$  thick wafer with soda lime glass cladding.

Figure 7 shows the Fourier transform of segments of the time-trace, permitting separation of the Si and silica contributions to the transmission based on arrival time. The figure clearly shows that the large pulses early in the time-trace had few high frequency components, as even fused silica will absorb high-frequency components over extended lengths, while the later part of the time-trace (associated with Si transmission) had a broader spectrum. This signal, with bandwidth out to  $\approx 4$  THz shows that we were able to couple into the 40  $\mu\text{m}$  thick Si, and not just



**Fig. 6.** Measurement of a fused silica clad 40  $\mu\text{m}$  Si slab. a) Fourier transform, b) Wigner-Ville transform, and c) time-trace, including pulses from the cladding modes.

the silica cladding. Practically all of the signal from 2 THz and above lies in the later part of the time-trace, proving that it passed through the high refractive index Si core. The sharp drop-off below 1 THz indicates significant reduction in transmission for the Si for the long wavelength components (related to the high silica attenuation and the theoretical cutoff for guided modes at 1.1 THz in the 40  $\mu\text{m}$  thick core).



**Fig. 7.** Fourier amplitudes of selected parts of the 40  $\mu\text{m}$  waveguide time trace.

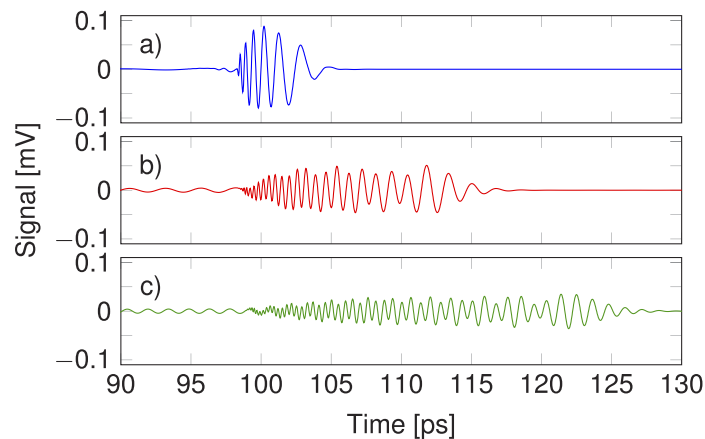
#### 4. Conclusion

We have successfully coupled into glass-clad Si slab waveguides of three thicknesses. The waveguides exhibit low attenuation and expected dispersion for the single-cycle pulses (frequency range 0.5 to 7.5 THz) when the core has a thickness of 160 or 300  $\mu\text{m}$ . Absorption differences for these samples are as anticipated by simulation results (see appendix). Despite coupling challenges, the expected spectral signature was also observed through a 40  $\mu\text{m}$  thick wafer with fused silica cladding. Silicon wafers of 40  $\mu\text{m}$  thickness are flexible, as are silicon-core fibers with

similar dimensions [36]. The broad transmission range of semiconductor core fibers would permit the exploration of dual-wavelength production and detection methods where phase-matching could be established by a suitable geometry. The observations in this paper provide guidance for future THz fiber production, as above 3 THz, dielectric guides are held to be the most realistic solution [13], with semiconductor core fibers as prime candidates.

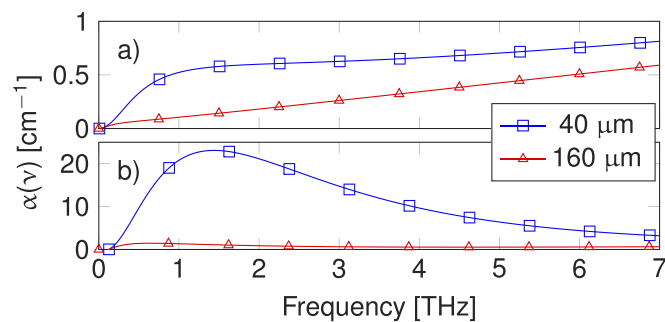
## Appendix

Figure 8 shows the time-trace of the fundamental mode and two higher order TE modes through a 160  $\mu\text{m}$  thick Si wafer with fused silica cladding. The difference in dispersion characteristics is quite evident, showing that the assumption of the fundamental mode dominating the transmission is reasonable.



**Fig. 8.** Time trace of the a) fundamental, b) secondary, and c) tertiary TE modes through a 160  $\mu\text{m}$  thick Si wafer with fused silica cladding

Figure 9 shows the calculated absorption coefficients for waveguides with 40 and 160  $\mu\text{m}$  thick Silicon cores with different claddings used in the simulations. When the core size is reduced, the impact of the absorptive cladding is greatly increased.



**Fig. 9.** Calculated absorption curves for 40 and 160  $\mu\text{m}$  thick Silicon cores. a) Fused silica cladding. b) Soda lime cladding.

## Funding

Norges Forskningsråd (262232); Vetenskapsrådet (2016-04488); Norges Teknisk-Naturvitenskapelige Universitet; Knut och Alice Wallenbergs Stiftelse (2016.0104).

## Disclosures

The authors declare no conflicts of interest.

## References

1. M. Tonouchi, "Cutting-edge terahertz technology," *Nat. Photonics* **1**(2), 97–105 (2007).
2. R. W. McGowan, G. Gallot, and D. Grischkowsky, "Propagation of ultrawideband short pulses of terahertz radiation through submillimeter-diameter circular waveguides," *Opt. Lett.* **24**(20), 1431–1433 (1999).
3. G. Gallot, S. P. Jamison, R. W. McGowan, and D. Grischkowsky, "Terahertz waveguides," *J. Opt. Soc. Am. B* **17**(5), 851–863 (2000).
4. R. Mendis and D. Grischkowsky, "Undistorted guided-wave propagation of subpicosecond terahertz pulses," *Opt. Lett.* **26**(11), 846–848 (2001).
5. K. Wang and D. M. Mittleman, "Metal wires for terahertz wave guiding," *Nature* **432**(7015), 376–379 (2004).
6. T.-I. Jeon, J. Zhang, and D. Grischkowsky, "THz sommerfeld wave propagation on a single metal wire," *Appl. Phys. Lett.* **86**(16), 161904 (2005).
7. A. Bingham, Y. Zhao, and D. Grischkowsky, "THz parallel plate photonic waveguides," *Appl. Phys. Lett.* **87**(5), 051101 (2005).
8. T.-I. Jeon and D. Grischkowsky, "THz zenneck surface wave (THz surface plasmon) propagation on a metal sheet," *Appl. Phys. Lett.* **88**(6), 061113 (2006).
9. S. P. Jamison, R. W. McGowan, and D. Grischkowsky, "Single-mode waveguide propagation and reshaping of sub-ps terahertz pulses in sapphire fibers," *Appl. Phys. Lett.* **76**(15), 1987–1989 (2000).
10. R. Mendis and D. Grischkowsky, "Plastic ribbon THz waveguides," *J. Appl. Phys.* **88**(7), 4449–4451 (2000).
11. H. Han, H. Park, M. Cho, and J. Kim, "Terahertz pulse propagation in a plastic photonic crystal fiber," *Appl. Phys. Lett.* **80**(15), 2634–2636 (2002).
12. M. Goto, A. Quema, H. Takahashi, S. Ono, and N. Sarukura, "Teflon photonic crystal fiber as terahertz waveguide," *Jpn. J. Appl. Phys.* **43**(2B), L317–L319 (2004).
13. C. Yeh, F. Shimabukuro, and P. H. Siegel, "Low-loss terahertz ribbon waveguides," *Appl. Opt.* **44**(28), 5937–5946 (2005).
14. L.-J. Chen, H.-W. Chen, T.-F. Kao, J.-Y. Lu, and C.-K. Sun, "Low-loss subwavelength plastic fiber for terahertz waveguiding," *Opt. Lett.* **31**(3), 308–310 (2006).
15. G. de los Reyes, A. Quema, C. Ponseca, R. Pobre, R. Quiroga, S. Ono, H. Murakami, E. Estacio, N. Sarukura, K. Aasaki, Y. Sakane, and H. Sato, "Low-loss single-mode terahertz waveguiding using cytop," *Appl. Phys. Lett.* **89**(21), 211119 (2006).
16. J. Carlito S. Ponseca, R. Pobre, E. Estacio, N. Sarukura, A. Argyros, M. C. Large, and M. A. van Eijkelenborg, "Transmission of terahertz radiation using a microstructured polymer optical fiber," *Opt. Lett.* **33**(9), 902–904 (2008).
17. K. Nielsen, H. K. Rasmussen, A. J. L. Adam, P. C. M. Planken, O. Bang, and P. U. Jepsen, "Bendable, low-loss topas fibers for the terahertz frequency range," *Opt. Express* **17**(10), 8592–8601 (2009).
18. V. Setti, L. Vincetti, and A. Argyros, "Flexible tube lattice fibers for terahertz applications," *Opt. Express* **21**(3), 3388–3399 (2013).
19. O. Mitrofanov and J. A. Harrington, "Dielectric-lined cylindrical metallic THz waveguides: mode structure and dispersion," *Opt. Express* **18**(3), 1898–1903 (2010).
20. M. Navarro-Cía, M. S. Vitiello, C. M. Bledt, J. E. Melzer, J. A. Harrington, and O. Mitrofanov, "Terahertz wave transmission in flexible polystyrene-lined hollow metallic waveguides for the 2.5-5 thz band," *Opt. Express* **21**(20), 23748–23755 (2013).
21. A. Malekabadi, S. A. Charlebois, D. Deslandes, and F. Boone, "High-resistivity silicon dielectric ribbon waveguide for single-mode low-loss propagation at f/g-bands," *IEEE Trans. Terahertz Sci. Technol.* **4**(4), 447–453 (2014).
22. K. Tsuruda, M. Fujita, and T. Nagatsuma, "Extremely low-loss terahertz waveguide based on silicon photonic-crystal slab," *Opt. Express* **23**(25), 31977–31990 (2015).
23. H. Amarloo and S. Safavi-Naeini, "Terahertz line defect waveguide based on silicon-on-glass technology," *IEEE Trans. Terahertz Sci. Technol.* **7**(4), 433–439 (2017).
24. M. Wächter, M. Nagel, and H. Kurz, "Metallic slit waveguide for dispersion-free low-loss terahertz signal transmission," *Appl. Phys. Lett.* **90**(6), 061111 (2007).
25. K. Mølster, "THz time domain spectroscopy of materials in reflection and transmission," Master's thesis, Department of Electronic Systems, Faculty of Information Technology and Electrical Engineering, NTNU (2017).
26. D. A. Bas, S. K. Cushing, J. Ballato, and A. D. Bristow, "Terahertz waveguiding in silicon-core fibers," (2013).
27. J. Ballato, T. Hawkins, P. Foy, R. Stolen, B. Kokuoz, M. Ellison, C. McMillen, J. Reppert, A. M. Rao, M. Daw, S. Sharma, R. Shori, O. Stafuss, R. R. Rice, and D. R. Powers, "Silicon optical fiber," *Opt. Express* **16**(23), 18675–18683 (2008).
28. N. Healy, M. Fokine, Y. Franz, T. Hawkins, M. Jones, J. Ballato, A. C. Peacock, and U. J. Gibson, "CO<sub>2</sub> laser-induced directional recrystallization to produce single crystal silicon-core optical fibers with low loss," *Adv. Opt. Mater.* **4**(7), 1004–1008 (2016).
29. Y. B. Ji, S. H. Kim, E. S. Lee, J. Son, and T. Jeon, "Development of optical fiber-coupled terahertz endoscope," in *2010 IEEE Photonics Society Winter Topicals Meeting Series (WTM)*, (2010), pp. 54–55.

30. X.-C. Zhang, "Terahertz wave imaging: horizons and hurdles," *Phys. Med. Biol.* **47**(21), 3667–3677 (2002).
31. M. Naftaly and R. E. Miles, "Terahertz time-domain spectroscopy of silicate glasses and the relationship to material properties," *J. Appl. Phys.* **102**(4), 043517 (2007).
32. M. Rubin, "Optical properties of soda lime silica glasses," *Sol. Energy Mater.* **12**(4), 275–288 (1985).
33. D. J. Cook and R. M. Hochstrasser, "Intense terahertz pulses by four-wave rectification in air," *Opt. Lett.* **25**(16), 1210–1212 (2000).
34. J. Dai, J. Zhang, W. Zhang, and D. Grischkowsky, "Terahertz time-domain spectroscopy characterization of the far-infrared absorption and index of refraction of high-resistivity, float-zone silicon," *J. Opt. Soc. Am. B* **21**(7), 1379–1386 (2004).
35. D. Grischkowsky, S. Keiding, M. van Exter, and C. Fattinger, "Far-infrared time-domain spectroscopy with terahertz beams of dielectrics and semiconductors," *J. Opt. Soc. Am. B* **7**(10), 2006–2015 (1990).
36. F. A. Martinsen, B. K. Smeltzer, J. Ballato, T. Hawkins, M. Jones, and U. J. Gibson, "Light trapping in horizontally aligned silicon microwire solar cells," *Opt. Express* **23**(24), A1463–A1471 (2015).